

## Article

# Acoustic Shooting and Bounce Ray Method for Calculating Echoes of Complex Underwater Targets

Gang Zhao <sup>1,2</sup>, Wei Zheng <sup>2</sup>, Naiwei Sun <sup>2</sup>, Shen Shen <sup>2</sup> and Xianyun Wu <sup>3,\*</sup> <sup>1</sup> School of Marine Science and Technology, Northwestern Polytechnical University, Xi'an 710060, China<sup>2</sup> Xi'an Precision Machinery Research Institute, Xi'an 710060, China<sup>3</sup> State Key Laboratory of Integrated Service Networks, Xidian University, Xi'an 710071, China

\* Correspondence: xywu@mail.xidian.edu.cn; Tel.: +86-29-8822-0310

**Abstract:** The acoustic scattering characteristics of a target are of great significance to the design of underwater acoustic detection systems. With the improvement in underwater weapon detection ability, the precision and accuracy of underwater target echo characteristic simulations are required to be higher and higher. The traditional underwater target simulation based on bright spot can no longer meet the needs of an underwater acoustic detection system for targeting fine feature recognition. This paper proposes a calculation using the fine complex underwater target echo bounce beam line method, in addition to the establishment of a bandwidth signal time domain calculation model and the integral dimension reduction to accelerate the algorithm on the basis of thorough target subspace division, combined with the geometrical acoustics method (GA) and physical acoustics (PA) for the pipeline space beam propagation tracking and aperture sound field to solve and realize the acoustic scattering characteristic calculation of a complex underwater target. Finally, the proposed method was verified by the Benchmark standard submarine. The accuracy and computational efficiency of the PA acceleration method are given, and the integrity of the target information calculated by the method is verified by acoustic ISAR imaging analysis. The simulation results show that the pipeline method of bouncing an acoustic beam is suitable for the simulation of complex underwater, target-wide band fine echoes.

**Keywords:** acoustic scattering characteristics of complex targets; acoustic shooting and bounce ray method; target wide band fine echo simulation



**Citation:** Zhao, G.; Zheng, W.; Sun, N.; Shen, S.; Wu, X. Acoustic Shooting and Bounce Ray Method for Calculating Echoes of Complex Underwater Targets. *Appl. Sci.* **2022**, *12*, 11707. <https://doi.org/10.3390/app122211707>

Academic Editor: Alessandro Ruggiero

Received: 10 October 2022

Accepted: 14 November 2022

Published: 17 November 2022

**Publisher's Note:** MDPI stays neutral with regard to jurisdictional claims in published maps and institutional affiliations.



**Copyright:** © 2022 by the authors. Licensee MDPI, Basel, Switzerland. This article is an open access article distributed under the terms and conditions of the Creative Commons Attribution (CC BY) license (<https://creativecommons.org/licenses/by/4.0/>).

## 1. Introduction

Modern and advanced submarines use technologies, such as the overall optimized design and surface noise reduction, which greatly reduces the scattering intensity of submarines to acoustic signals. At the same time, with the development of underwater acoustic countermeasure equipment, the simulation of underwater scale targets and even volume targets have become a possibility, and all of these pose significant challenges for underwater target detection [1].

At present, acoustic waves are still the main means of underwater target detection, but the traditional underwater target simulation echoes based on the bright spot theory contain limited information and cannot express more detailed acoustic characteristics of the targets [2]. How to realize the precise simulation of the complex underwater target echo and to greatly improve the information integrity of the echo in the time–space frequency domain has become an important area of current research [3,4].

## 2. Frequency Domain Scattered Sound Field Modeling

The surfer space position relationship is shown in Figure 1.

The *S* point is the target geometric center point and the origin of the basic coordinate system, *Q* point is the position of the co-located sound source used for sending and

receiving, and  $\mathbf{r}$  represents the coordinate origin  $S$  in the basic coordinate system to the sound source (receiving) point  $Q$  vector.

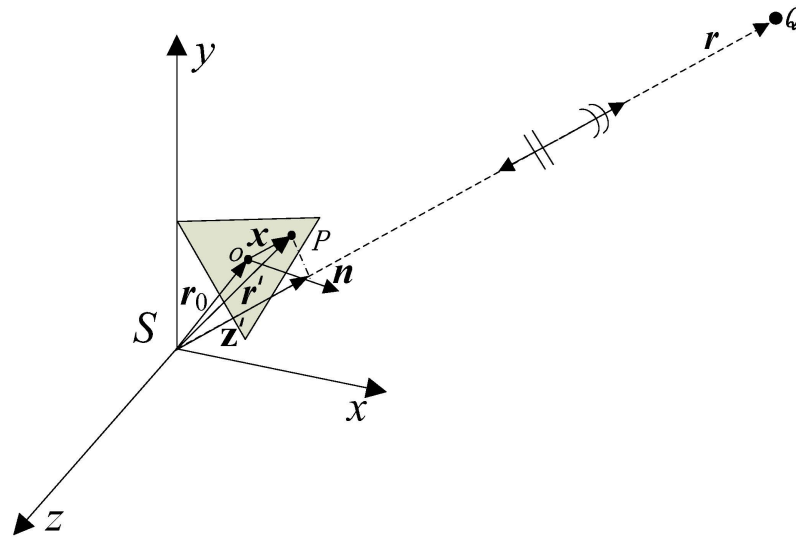


Figure 1. Time domain discrete integral acceleration algorithm object.

Point  $O$  is the geometric center of any surface element on the target surface,  $\mathbf{n}$  is the normal vector of the surface element, and  $\mathbf{r}_0$  represents the vector from the coordinate origin to the center point of the surface element in the basic coordinate system;

Point  $P$  is any point on the surface element, and  $\mathbf{x}$  represents the vector from the geometric center of the element under the basic coordinate system from point  $O$  to point  $P$ ,  $\mathbf{r}'$  represents the vector from the coordinate origin  $S$  to point  $P$  in the basic coordinate system, and  $\mathbf{z}'$  represents the projection of  $\mathbf{r}'$  to  $\mathbf{r}$  vector.

The Kirchhoff integral formula in the frequency domain in the far-field is as follows:

$$P_s(\mathbf{r}, \omega) = -\frac{ik}{2\pi r} e^{-ikr} \iint_S \Gamma(\phi) e^{ikz'} P_i(\mathbf{r}', \omega) \cos\phi dS \tag{1}$$

where  $P_s(\mathbf{r}, \omega)$  is the frequency response of the target scattered sound field at any field point determined by the space vector  $\mathbf{r}$ .  $P_i(\mathbf{r}', \omega)$  is the frequency response of the incident sound field at any position vector  $\mathbf{r}'$  on the target surface.  $G(\mathbf{r}, \mathbf{r}', \omega)$  is the Green's function, and  $\frac{\partial G(\mathbf{r}, \mathbf{r}', \omega)}{\partial n}$  is the partial differential of the Green's function normal to the target surface [5,6].

Under far-field conditions,  $r \rightarrow \infty$ , then the Green's function  $G(\mathbf{r}, \mathbf{r}', \omega)$  satisfies the following approximation:

$$G(\mathbf{r}, \mathbf{r}', \omega) = \frac{e^{-ik_i \cdot (\mathbf{r} - \mathbf{r}')}}{4\pi|\mathbf{r} - \mathbf{r}'|} \approx \frac{e^{-ik_i r}}{4\pi r} e^{ik_i \cdot \mathbf{r}'} \tag{2}$$

then:

$$\frac{\partial G(\mathbf{r}, \mathbf{r}', \omega)}{\partial n} \approx -(ik_i + \frac{1}{r}) \cos\phi_i G(\mathbf{r}, \mathbf{r}', \omega) \approx -ik_i \cos\phi_i G(\mathbf{r}, \mathbf{r}', \omega) \tag{3}$$

where  $\mathbf{k}_i = \mathbf{r}/r$  is the incident wave-front vector, and  $\phi_i$  is the angle between the incident wave-front vector  $\mathbf{k}_i$  and the surface element normal vector  $\mathbf{n}$ .

Let  $P_i(\mathbf{r}', \omega)$  denote the incident sound pressure at any point  $P$  on the target surface represented by the vector  $\mathbf{r}'$ ,  $P_i(\mathbf{r}_0, \omega)$  denote the incident sound pressure at the geometric center  $O$  of the target surface represented by the vector  $\mathbf{r}_0$ , and  $P_s(\mathbf{r}', \omega)$  denote the scattered sound pressure on the target surface at any point  $P$  represented by the vector  $\mathbf{r}'$ .  $E$  is the

angle between the backscattered wavefront vector  $\mathbf{k}_s = (\mathbf{r} - \mathbf{r}') / (r - r')$  and the normal vector  $\mathbf{n}$ .

As the far-field condition  $r \rightarrow \infty$  is satisfied under the co-location of the transceiver, there are  $\phi_i \approx \phi_s = \phi$ ,  $\mathbf{k}_i \approx -\mathbf{k}_s$ ,  $\mathbf{k}_i \cdot \mathbf{r}' = z'$ ,  $\mathbf{k}_i \cdot (\mathbf{r} - \mathbf{r}') = r - z'$  (that is, the projection of the vector  $\mathbf{r} - \mathbf{r}'$  on the vector  $-\mathbf{k}_i$ ).

Considering the scale of the panel itself  $l \ll r \rightarrow \infty$ , it is reasonable to use  $P_i(\mathbf{r}_0, \omega)$  to represent the sound pressure value of the entire panel. What needs to be changed is the phase of the panel, and the change in the phase is reflected by  $\exp(i\mathbf{k}_i \cdot (\mathbf{r} - \mathbf{r}'))$ .

According to the above conditions, the following formulas can be obtained:

$$P_i(\mathbf{r}', \omega) \approx P_i(\mathbf{r}_0, \omega)e^{i\mathbf{k}_i \cdot \mathbf{r}'} \tag{4}$$

$$\frac{\partial P_i(\mathbf{r}', \omega)}{\partial n} \approx -ik_i \cos \phi_i P_i(\mathbf{r}', \omega) \approx -ik_i \cos \phi_i P_i(\mathbf{r}_0, \omega)e^{i\mathbf{k}_i \cdot \mathbf{r}'} \tag{5}$$

$$P_s(\mathbf{r}', \omega) \approx \Gamma(\phi)P_i(\mathbf{r}', \omega) \approx \Gamma(\phi)P_i(\mathbf{r}_0, \omega)e^{i\mathbf{k}_i \cdot \mathbf{r}'} \tag{6}$$

$$\frac{\partial P_s(\mathbf{r}', \omega)}{\partial n} \approx -\Gamma(\phi)\frac{\partial P_i(\mathbf{r}', \omega)}{\partial n} \approx ik_i \cos \phi_i \Gamma(\phi)P_i(\mathbf{r}_0, \omega)e^{i\mathbf{k}_i \cdot \mathbf{r}'} \tag{7}$$

where  $\Gamma(\phi)$  is the reflection coefficient, which can be obtained according to the layered medium acoustic definition regardless of whether the target surface is rigid or not at a high frequency approximation.

Substitute the non-approximate scheme of Equation (2) into Equation (1), and simplify Equation (1) by using  $-\mathbf{k}_i \cdot (\mathbf{r} - \mathbf{r}') = r - z'$ , and  $\mathbf{k}_i \cdot \mathbf{r}' = z'$ , then the scattered sound pressure at  $\mathbf{r}$ ,  $P_s(\mathbf{r}, \omega)$  can be written as:

$$P_s(\mathbf{r}, \omega) = -\frac{ik}{2\pi r} e^{-ikr} \iint_S \Gamma(\phi) e^{ikz'} P_i(\mathbf{r}', \omega) \cos \phi dS \tag{8}$$

The scattered field is divided into surface elements of the target surface for discrete integration:

$$P_{ss}(\mathbf{r}, \omega) = -\frac{ik}{2\pi r} e^{-ikr} \sum_{m=1}^M \Gamma_m(\phi_m) \iint_{S_m} e^{ikz'} P_i(\mathbf{r}_i, \omega) \cos \phi_m dS \tag{9}$$

or

$$P_{ss}(\mathbf{r}, \omega) = -\frac{ik}{2\pi r} P_i(\mathbf{r}_0, \omega) e^{-ikr} \sum_{m=1}^M \Gamma_m(\phi_m) \iint_{S_m} e^{2ikz'} \cos \phi_m dS$$

$P_{ss}(\mathbf{r}, \omega)$  represents the total scattered sound field in the target frequency domain,  $M$  represents the total number of surface elements on the target surface,  $\Gamma_m(\phi_m)$  represents the reflection coefficient of surface elements,  $S_m$  represents the region of each surface element, and  $\phi_m$  represents the angle between the normal vector  $\mathbf{n}$  on each surface element.

### 3. Modeling of Time-Domain Scattered Sound Field

Equation (9) can be used to calculate the sound field characteristics of a single frequency signal in the frequency domain, but it is not suitable for a wide band signal system. Fourier transform is applied to Equation (8) to obtain the time-domain sound field model [7,8]:

$$\begin{aligned}
 p_s(\mathbf{r}, t) &= \frac{1}{2\pi} \int_{-\infty}^{\infty} P_s(\mathbf{r}, \omega) e^{i\omega t} d\omega \\
 &= \frac{1}{2\pi} \int_{-\infty}^{\infty} \left\{ -\frac{ik}{2\pi r} e^{-ikr} \iint_S \Gamma(\phi) e^{ikz'} P_i(\mathbf{r}', \omega) \cos\phi dS \right\} e^{i\omega t} d\omega \\
 &= \frac{1}{2\pi rc} \iint_S \Gamma(\phi) \left\{ \frac{1}{2\pi} \int_{-\infty}^{\infty} P_i(\mathbf{r}', \omega) \frac{\partial}{\partial t} e^{i\omega(t-\frac{r-z'}{c})} d\omega \right\} \cos\phi dS \\
 &= -\frac{1}{2\pi rc} \iint_S \Gamma(\phi) \frac{\partial}{\partial t} \left\{ \frac{1}{2\pi} \int_{-\infty}^{\infty} P_i(\mathbf{r}', \omega) e^{i\omega(t-\frac{r-z'}{c})} d\omega \right\} \cos\phi dS \\
 &= -\frac{1}{2\pi rc} \iint_S \Gamma(\phi) \frac{\partial}{\partial t} \left\{ \frac{1}{2\pi} \int_{-\infty}^{\infty} P_i(\mathbf{r}_0, t - \frac{r-2z'}{c}) \right\} \cos\phi dS
 \end{aligned} \tag{10}$$

The following formula can be used to calculate the partial time conductance of the time domain sound field:

$$\frac{\partial}{\partial t} \{P_i(\mathbf{r}_0, t)\} = \frac{P_i(\mathbf{r}_0, t - \Delta t) - P_i(\mathbf{r}_0, t + \Delta t)}{2\Delta t} \tag{11}$$

where  $\Delta t$  represents the discretization of time.

Similarly, the time domain scattering field is divided into the surface elements of the target surface for discrete integration:

$$P_{ss}(\mathbf{r}, t) = -\frac{1}{4\pi rc \Delta t} \sum_{m=1}^M \Gamma_m(\phi_m) \iint_{S_m} (P_i(\mathbf{r}_0, t - \frac{r-2z'}{c} - \Delta t) - P_i(\mathbf{r}_0, t - \frac{r-2z'}{c} + \Delta t)) \cos\phi_m dS \tag{12}$$

When using Equation (12) to calculate the time-domain signals of the sound field, time discrete sampling is required, and the frequency change process of the wideband signal is expressed by the time function. Therefore, time discrete sampling also realizes the solution of the time-domain sound field characteristics of the wide band signal, and the specific process is described in the following section.

#### 4. Dimension Reduction by Time Domain Integration

In general, many plane or surface integrals are required to obtain the time-domain results of the scattered field, which has high computational complexity. Thus, it needs to be accelerated by integration.

Taking the single-frequency signal as an example, the expression of the incident acoustic wave without considering the initial phase is  $P_i = \exp(i2\pi f_0 t)$ . Considering the motion of the target, without calculating the micro-Doppler generated by the projection relation, etc., the form of the target echo is  $P_r = \exp(i2\pi f_d t)$ , where:

$$\begin{aligned}
 f_d &= f_0 \sigma \\
 \sigma &= \frac{1 + V_m/C}{1 - V_m/C}
 \end{aligned} \tag{13}$$

$f_d$  represents the Doppler center frequency of the target echo signal;  $f_0$  represents the center frequency of the incident acoustic signal;  $\sigma$  stands for the Doppler factor;  $V_m$  represents the relative projection velocity of the target; and  $C$  is the speed of sound in water.

Then, the surface integral part in Equation (12) can be expressed as follows:

$$\begin{aligned}
 &\iint_{S_m} (P_i(\mathbf{r}_0, t - \frac{r-2z'}{c} - \Delta t) - P_i(\mathbf{r}_0, t - \frac{r-2z'}{c} + \Delta t)) \cos\phi_m dS \\
 &= (e^{i2\pi f_0(t-\frac{r}{c}-\Delta t)} - e^{i2\pi f_0(t-\frac{r}{c}+\Delta t)}) \cos^2\phi_m \iint_{S_m} e^{i2\pi f_0(\frac{2z'}{c})} dS
 \end{aligned} \tag{14}$$

As shown in Figure 1, considering that  $z'$  is the modulus value of the vector projected by  $\mathbf{r}'$  to  $\mathbf{r}$ , and according to the definition of vector  $\mathbf{r}_0$  and  $\mathbf{x}$ ,  $z'$  can be expressed as:

$$z' = (\mathbf{r}_0 + \mathbf{x}) \cdot \frac{\mathbf{r}}{|\mathbf{r}|} = (\mathbf{r}_0 + \mathbf{x}) \cdot \frac{\mathbf{r}}{r} \tag{15}$$

Substitute Equation (14) into Equation (13), where the surface integral part is rewritten as:

$$\iint_{S_m} e^{i2\pi f_0(\frac{2z'}{c})} dS = e^{i4\pi\frac{f_0}{c}(\mathbf{r}_0 \cdot \frac{\mathbf{r}}{r})} \iint_{S_m} e^{i4\pi\frac{f_0}{c}(\mathbf{x} \cdot \frac{\mathbf{r}}{r})} dS \tag{16}$$

Let  $k = 2\pi f_0/c$  and  $K = 2k$ , and let  $\mathbf{u}$  be the projection vector of vector  $\mathbf{r}/r$  on  $S_m$ , namely:  $\mathbf{u} = \mathbf{r}/r - (\mathbf{r}/r \cdot \mathbf{n})\mathbf{n}$ . According to the vector relationship, we can know:  $\mathbf{x} \cdot \mathbf{u} = \mathbf{x} \cdot [\mathbf{r}/r - (\mathbf{r}/r \cdot \mathbf{n})\mathbf{n}] = \mathbf{x} \cdot \mathbf{r}/r$ .

After  $\mathbf{x} \cdot \mathbf{r}/r$  in Equation (16) is replaced by  $\mathbf{x} \cdot \mathbf{u}$ , the Stokes formula condition is satisfied, then the final dimensionality reduction form of Equation (12) is:

$$\begin{aligned} P_{ss}(\mathbf{r}, t) &= -\frac{1}{4\pi rc \Delta t} \sum_{m=1}^M \Gamma_m(\phi_m) \iint_{S_m} (P_i(\mathbf{r}_0, t - \frac{r - 2z'}{c} - \Delta t) - P_i(\mathbf{r}_0, t - \frac{r - 2z'}{c} + \Delta t)) \cos\phi_m dS \\ &= -\frac{1}{4\pi rc \Delta t} \sum_{m=1}^M \Gamma_m(\phi_m) (e^{i2\pi f_0(t - \frac{r}{c} - \Delta t)} - e^{i2\pi f_0(t - \frac{r}{c} + \Delta t)}) \cos^2\phi_m e^{iK(\mathbf{r}_0 \cdot \frac{\mathbf{r}}{r})} \\ &\quad \cdot \frac{i}{Ku^2} \sum_{n=1}^N (\mathbf{u}^* \cdot \Delta \mathbf{a}_n) \text{sinc}(Ku \cdot \Delta \mathbf{a}_n / 2) \exp[iKu \cdot (\mathbf{a}_{n+1} + \mathbf{a}_n) / 2] \end{aligned} \tag{17}$$

For the specific derivation of Equation (16), please refer to Gordon’s integral derivation process [9]. When Equation (16) is used to solve the target time-domain scattered sound field, only the discrete sum calculation is required instead of the two-dimensional integration, which greatly reduces the computational complexity.

For the LFM signal:

$$P_i = \exp(i\pi(ft + Kt^2/2)) \tag{18}$$

where  $K$  is the frequency modulation slope. As  $\mathbf{T} = (t_1, t_2, \dots, t_m, t_{m+1}, \dots, t_n)$  is a time sampling sequence with interval  $\delta t$ ,  $T_0 = 0$  is the initial time of the pulse, then:

$$P_i(\mathbf{T}) = \exp(i\pi(f\mathbf{T} + K\mathbf{T}^2/2)) \tag{19}$$

Note that the LFM echo signal is in the form of:

$$P_r = \exp(i\pi(f\sigma t + K\sigma^2 t^2/2)) \tag{20}$$

For any time sampling point  $t_m$ ,  $F = ft_m + K\sigma^2 t_m^2/2$ , then  $P_r(t_m) = \exp(i\pi F)$ .

Since the dimensionality reduction object of Equation (17) is the far-field incident acoustic range difference and its transformation result, each  $P_r(t_m)$  can be regarded as a single frequency signal, and the dimensionality reduction solution can also be performed using the method in Equation (17) [10].

### 5. Acoustic Shooting and Bounce Ray Method

In the Kirchhoff approximation problem of the meshing surface elements, the total target echo is solved on the basis of solving the acoustic scattering of each independent surface element. The key to the problem lies in the calculation of the integral of surface elements, and the judgment and treatment of the occlusion and reflection relationship of the complex surface of the target under the conditions of acoustic wave incidence [7,11]. The bandwidth signal time domain calculation formula was deduced and accelerated the algorithm to realize efficiency for the large panel acoustic scattering problem to solve; in this paper, it is the GA PA bounce sound underwater target scattering characteristics of the acoustic radiation calculation method (ASBR, Acoustic Shooting and Bounce Ray) [12,13].

As shown in Figure 2, the beam aperture surface is defined in the front direction of the incoming acoustic wave of the target, and the beam pipeline is divided according to certain accuracy requirements. Each beam pipeline consists of four vertices and a tracking point. By dividing the subspace of the target surface and tracing the space propagation of each acoustic beam pipeline, the intersection and reflection relationship between the pipeline and the target surface element are calculated to complete the GA calculation. The PA sound field integration is also carried out on the surface element, where it meets the ejection condition, so as to realize the calculation of the acoustic scattering characteristics of underwater target combined with GA and PA [14].

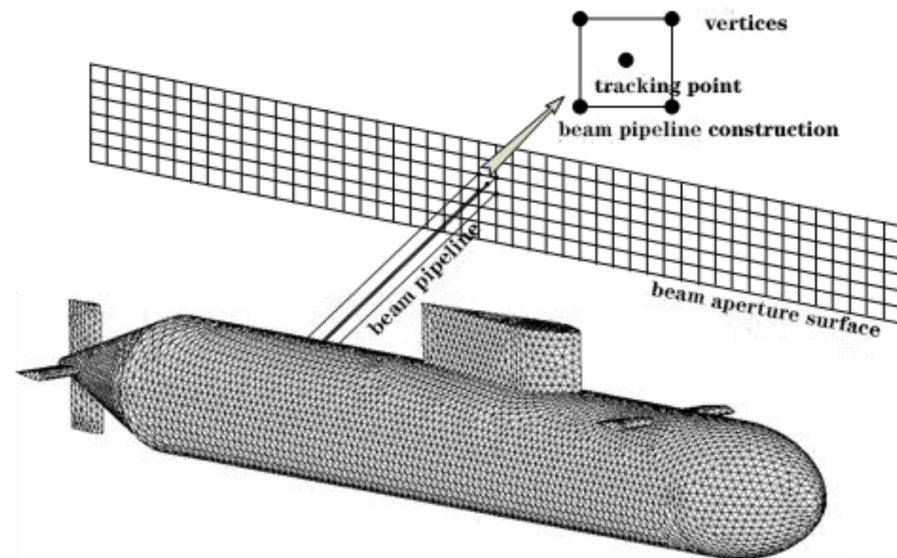


**Figure 2.** Beam aperture surface and beam pipeline definition.

Based on the natural attribute, the parallel GA process on the exit surface yuan, according to Equation (9) for the time domain integral, and the PA process of the all beam line can be used in a fully parallel manner, the computing environment can select the nucleus, the blade array, as well as the GPU cluster. Thus, the high performance parallel platform and implementation of the parallel algorithm design and deployment are not discussed in this paper. In addition, the implementation of the ASBR method also needs to consider the following key issues about the acoustic beam pipeline tracking process, which have a direct impact on the performance of the algorithm

### 5.1. Target Subspace Division

The underwater target detection process of the acoustic pulse is greatly affected by the hydrological environment. In general, there will be multiple intrinsic acoustic beams that irradiate to the target with different incidence angles and arrival times. However, considering that the aperture plane scale of the beam along the horizontal direction of the target will be more different, and the incident deviation angle in the vertical direction can be processed by the intersection of the line and plane traced by the beam pipeline. Therefore, the division of the target subspace takes the geometric center of the target as the coordinate origin and is constructed according to the geodetic coordinate system, as shown in Figure 3 [15].

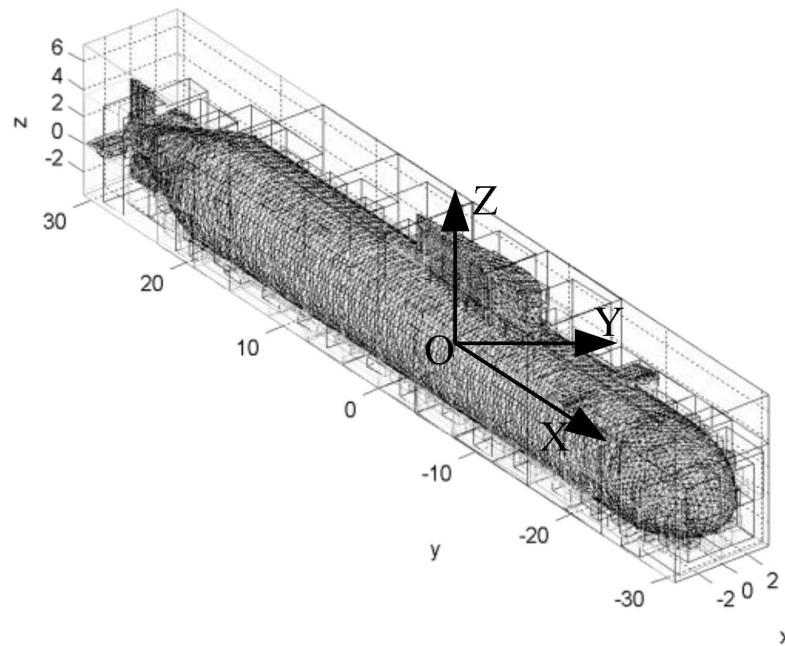


**Figure 3.** Object subspace partition schematic.

The subspace partition algorithm is based on the KD-tree space partition of the size nodes based on SAH, and it is realized by the pipeline tracing of the rope-KD sound beam without stack.

5.2. Intersection Test between Acoustic Beam Pipeline and Plane Triangular Plane Element

After tracing the acoustic beam pipeline to the interior of the target subspace, it needs to perform the intersection test with the target surface element. This process can be regarded as a confirmation of the relationship between the intersection point and the target surface element position [16].

As shown in Figure 4, the ray  $P = P_0 + tU$  originating from the tracking point  $O'$  of the space acoustic beam pipeline has an initial position vector of  $P_0$  and a direction vector of  $U$ . After traveling a distance of  $t_c$  along the direction of  $U$ ,  $O'$  intersects with the triangular plane element  $S_0$  on the target surface with point  $V_c$ . Given the coordinates of the three vertices  $V_0, V_1$  and  $V_2$  of the triangular plane element, confirm whether  $V_c$  is in the  $S_0$  plane, and it can actually be transformed into the problem of judging the position the relationship between  $V_c$  and the three vertices and triangle sides, namely for point  $V_2$ , determine whether  $V_c$  and  $V_2$  are on the same side of edge  $V_0 V_1$ . Similarly, determine the positions of points  $V_0, V_1$  and  $V_2$ . If they all meet the same side relationship, then  $V_c$  is in the  $S_0$  plane. Similarly, determine the positions of points  $V_0, V_1$  and  $V_2$ . If they all meet the same side relationship, then  $V_c$  is in the  $S_0$  plane.

Using the vector operation property, the above judgment is expressed as:

$$\begin{cases} \text{if } \prod_{i=0}^{k-1} \{ (\overrightarrow{V_c V_i} \times \overrightarrow{V_i V_{i+1}}) \cdot (\overrightarrow{V_{i+2} V_i} \times \overrightarrow{V_i V_{i+1}}) \} > 0 & V_c \in S_0 \\ \text{else } & V_c \notin S_0 \end{cases} \quad n = n \bmod k \quad (21)$$

In the formula,  $k = 3; n = i, i + 1, i + 2$  in all the lower indices.

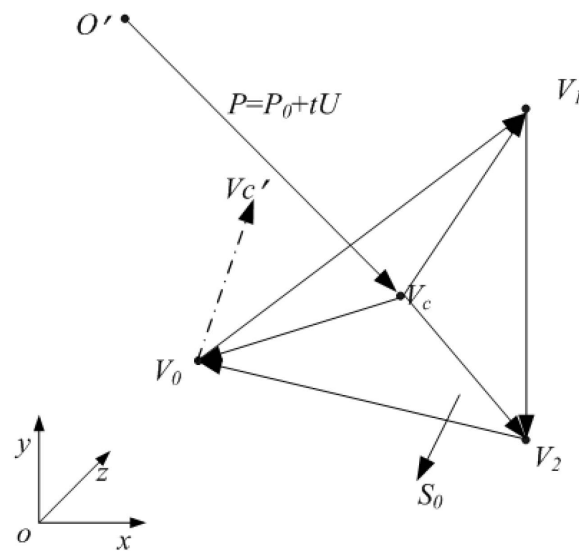


**Figure 4.** Schematic diagram of the intersection of the acoustic beam pipeline and triangular plane element.

### 5.3. Triangular Plane Element Occlusion Judgment

From the relative position relationship of the plane elements, following situations as shown in Figure 5.

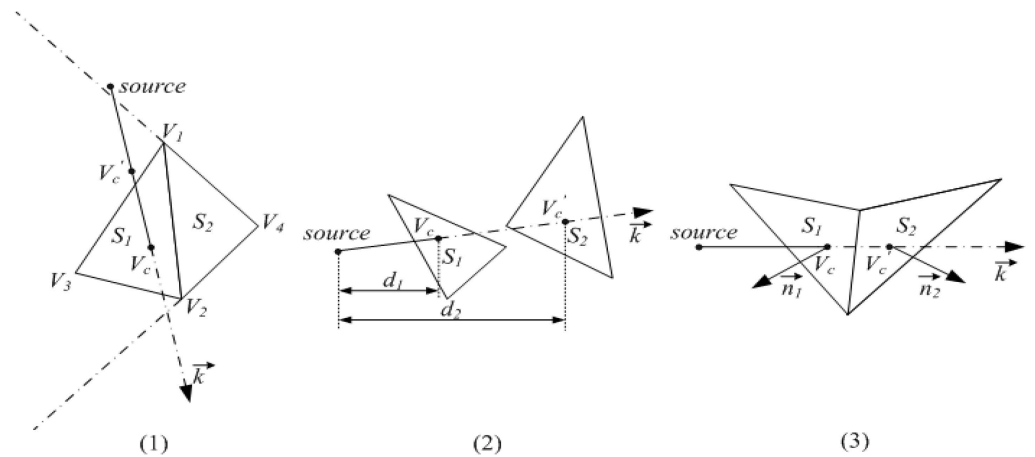


**Figure 5.** Several methods of surface element occlusion: (1) No occlusion Case; (2) Non-adjacent occlusion case; (3) Adjacent occlusion case.

From case (1) in the figure, the intersection calculation of the ray and the triangular plane element mentioned above can be judged. In case (2), the occlusion judgment needs to calculate the distance  $d_1$  and  $d_2$  between the intersection point of  $\vec{k}$ ,  $S_1$  and  $S_2$  and the source point to judge the occlusion situation.

In the subspace partition of the KD-tree, the most likely situation is (3). In this case, we can judge the relation between the angle between  $\vec{k}$  and the normal vector of the plane element. When the angle is obtuse, it intersects and the acute angle is occluded. Namely:

$$\text{if } \vec{k} \cdot \vec{n} < 0 \text{ Irradiated surface else occluded surface.}$$

### 5.4. Acoustic Beam Pipeline Strength Tracking

Under the condition of medium- and high-frequency acoustic wave incidence, although all the irradiated surfaces produce the target's backward acoustic scattering, the last

irradiated surface contributes the most. There is little difference between the PA calculation on all the surfaces and the calculation only on the last irradiated surface [17]. In this case, the  $i$  intersection point  $r_i$  ( $i = 1, 2, \dots, N$ ). If the field strength  $\Phi(r_i)$  is known, then the field strength at the  $i + 1$  intersection point  $r_{i+1}$  is:

$$\Phi(r_{i+1}) = D_{r_i} \cdot \Gamma_{r_i}(\phi) \cdot \Phi(r_i) \cdot e^{-jk|r_{i+1}-r_i|} \tag{22}$$

In the formula,  $\Gamma_{r_i}(\phi)$  is the acoustic reflection coefficient at the intersection  $r_i$ , which can be defined as in Equation (7) according to Snell’s theorem of layered media acoustics. When the target is a rigid external surface,  $\Gamma_{r_i}(\phi) = 1$ ;  $D_{r_i}$  is the diffusion factor at the intersection  $r_i$ . When plane elements are used to mesh the target surface,  $D_{r_i}$  is set as 1.

5.5. Acoustic Beam Pipeline Splitting Processing

When the vertex method is used to track the acoustic beam pipeline in space, the special case of intersecting with discontinuous target surface elements is excluded, and the acoustic beam pipeline incident on different target surface elements needs to be split. In the case of the plane wave incident, the results of the acoustic field integration of a plane element is only related to the integrated area and has nothing to do with the particle size of the plane element. Therefore, a local analysis of the acoustic beam pipeline to be split is shown in Figure 6.

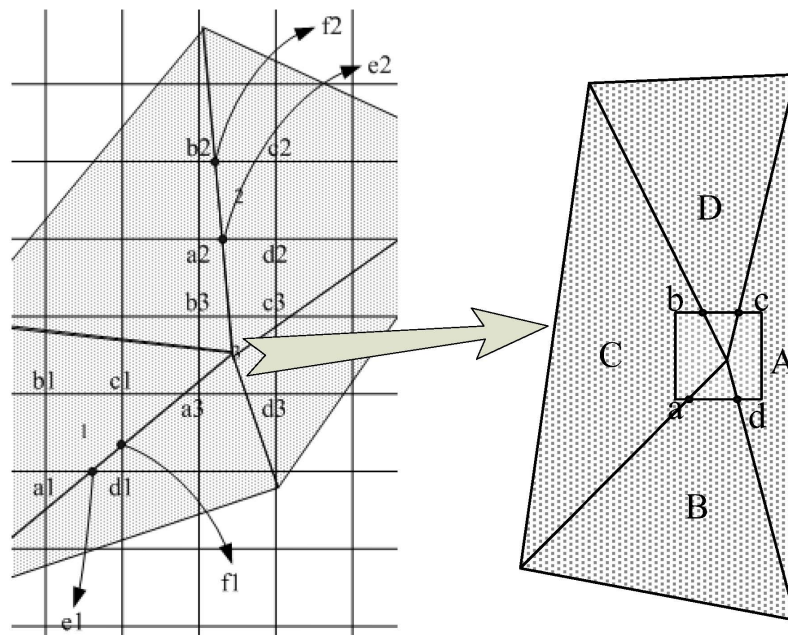


Figure 6. Local and special cases of the intersection between the plane element and acoustic beam.

According to the intersection of the acoustic beam pipeline and target surface element in Figure 6, various splitting definitions are given as follows:

- (1) If three of the four vertices of the acoustic beam pipeline fall on the same target surface element and the remaining one falls on the other target surface element, it is called type I splitting, as shown in Figure 6 for pipeline No. 1;
- (2) If the four vertices of the acoustic beam pipeline fall on two target surface elements in pairs, it is called type II splitting, as shown in Figure 6 for pipeline No. 2;
- (3) If the four vertices of the acoustic beam pipeline fall in more than three different target surface elements, it is called type III splitting, as shown in Figure 6 for pipeline No. 3.

The serial number of the target surface element intersecting the four corner tops of the pipeline is recorded, respectively, during the line and surface intersection test, and the

pipeline splitting type can be obtained and processed through the above judgment. The process is as follows:

- (1) If a pipeline has type I splitting, the pipeline must only intersect with two target surface elements. The intersection points E1 and F1 can be further solved by corner coordinates. The sound field integration is directly carried out on the pentagon plane (A1B1C1F1E1 in Figure 6) and the triangle plane (D1E1F1 in Figure 6).
- (2) If type II splitting occurs in a pipeline, the intersection point between the pipeline and the target surface element can be further solved by corner coordinates. If there are only two intersection points of E2 and F2 in Figure 6, then the pipeline must only intersect with two target surface elements, which is defined as type II-1 splitting. The sound field integration is directly carried out on two quadrilateral planes (A2B2F2E2 and C2D2E2F2 in Figure 6). If there are more than two intersections, it is defined as a type II-2 split and is treated in the same way as a type III split.
- (3) If a line of four horns falls in three or more graphics, define it as a type III division, and the actual fellowship with the plane cannot be launched directly from the angle of the point coordinates (in Figure 3, the line is down to the four plane); an evenly divided line will be required before the split type judgment and handling;
- (4) If a pipeline has been split several times to reach the set aperture accuracy and it still belongs to type II-2 or III split, it will be discarded.

In the actual calculation, type I and Type II-1 are the most important types of split pipelines, which do not require a uniform subdivision of pipeline aperture except for the distributed calculation of the sound field integration. Type III splitting occurs at the center of each grid and is the main source of uniform splitting pipelines. However, the occurrence probability of type II-2 splitting is very low. In order to improve the computational efficiency, the method of direct discard can be adopted.

## 6. PA Calculation Is Accelerated

In the ASBR method, after the intersection and reflection judgment of the acoustic beam pipeline of GA, and after the target surface element is completed, the final PA calculation needs to be completed on the aperture plane of the acoustic beam pipeline. Equation (16) can be used to complete the integral dimension reduction of the aperture surface element. It is noted that, when  $u = 0$ , that is, when the observation point vector coincides with the incident wave vector, the calculation result of the integral formula of Equation (16) is numerically reduced to the S0 area of the aperture plane element. In this case, the incident wave vector is perpendicular to the integrated aperture plane element, and the sound path difference at all points on the aperture plane element is 0.

For the common plate element method, since the integration is carried out on the target surface element, the granularity of the surface element partition will directly determine the accuracy of the sound field solution and has a great impact on computational efficiency. For these reasons, the granularity of the surface element division is generally keener  $\ll 1 \lambda$  when solving the acoustic scattering problem of large underwater targets. In this case, the time-domain integral formula must be solved normally, otherwise it will cause a large calculation error. However, in the ASBR method, the integration is performed on the aperture surface of the acoustic beam pipeline. When the target surface elements are divided according to a certain granularity, the algorithm accuracy is mainly determined by the granularity of the acoustic beam pipeline on the equivalent aperture surface. Since the realization process of the ASBR method naturally has a high parallelism of the beam pipeline as a unit, using high-performance parallel computing capability means that the aperture division granularity of the conventional underwater target can be  $\geq 0.1 \lambda$  or smaller. In this case, the acoustic path difference in the integral formula of Equation (16) will also be constrained in a small range. On the premise of sacrificing a certain solution accuracy, the pipeline acoustic beam aperture plane can be regarded as an independent isophase plane, thus eliminating the plane integral solution process in Equation (16). This therefore improves the solution efficiency of the ASBR method.

## 7. Simulation Evaluation

### 7.1. Simulation Calculation Condition

The computational conditions of the simulation example used in this paper are as follows: Sound velocity  $C = 1500$  m/s; in the case of scavenging, the incident wave has a CW signal center frequency  $f_c = 15$  KHz, LFM signal center frequency  $f_c = 15$  KHz, and frequency slope  $K = 10$  KHz/s. The signal pulse width  $\tau = 10$  ms and the other pulses  $\tau = 70$  ms. The model parameters used in the calculation are shown in Table 1. To ensure the calculation accuracy and solving efficiency, the surface meshing aperture of the ball, cylinder and cross column is  $0.5 \lambda$  (0.05 m). The surface meshing aperture of the Benchmark submarine is  $2 \lambda$  (0.2 m) because of its large size.

**Table 1.** Description of calculation model.

Model Type	Sphere	Cylindrical	Cross Column	Benchmark
The model size	Radius 1 m/5 m	Radius 1.5 m Length 10 m	Radius 1.5 m Length 10 m (Center cross)	Length 65.0 m Width 7.5 m High: 11.0 m
Surface mesh aperture	$0.5 \lambda$ (0.05 m)/ $2 \lambda$ (0.2 m)	$0.5 \lambda$ (0.05 m)	$0.5 \lambda$ (0.05 m)	$2 \lambda$ (0.2 m)
Bin number	11,636/18,252	68,670	157,342	132,040

Due to the natural parallelism characteristic of the TD-ASBR method proposed in this paper, all model simulation calculations are carried out based on the NvidiaTeslaP100GPU computing acceleration card array, and the theoretical parallel computation force of the GPU computing array is 95TFLOPS. In fact, due to the parallel computing cost, there is approximately 70 TFLOPS~85 TFLOPS.

Preparation for the target echo simulation:

- (1) Preparation for importing model mathematical modeling results in grid division software to complete grid subdivision;
- (2) Preparation: Import the segmented surface topology data to the time domain echo simulation software;
- (3) Preparation for selection of computing resources and setting of scanning mode and initial simulation setting parameters;
- (4) Start simulation echo calculation: After preparation for the next calculation, I used a high-speed network to store the simulation results locally in the required format and released the simulation resources.

### 7.2. Algorithm Validation

The verification of the simulation algorithm is carried out from the perspective of correctness, effectiveness and information completeness by using the main sphere, cylinder and other standard models. At the same time, the classical mathematical model is used to verify its engineering applicability.

- (a) Verify the correctness

The sphere and cylinder model with a radius of 1 m shown in Table 1 were taken as objects to verify the correctness of the algorithm. The aperture of the acoustic beam pipeline was set as 0.005 m, plane angle scanning was carried out on the sphere model, and plane frequency scanning was carried out on the cylinder model on the orthogonal surface of the cylinder. The comparison between the model target intensity results obtained by the simulation and the theoretical analytical values was shown in Figures 7 and 8. As can be seen from the figure, under the conditions of a sweep angle and sweep frequency, the deviation between the simulation results of the target strength of the standard model and the theoretical analytical values is less than 3 dB (as demonstrated by the mid-point line

and the break line in the figure), and has a good consistency, which proves the correctness of the TD-ASBR simulation algorithm.

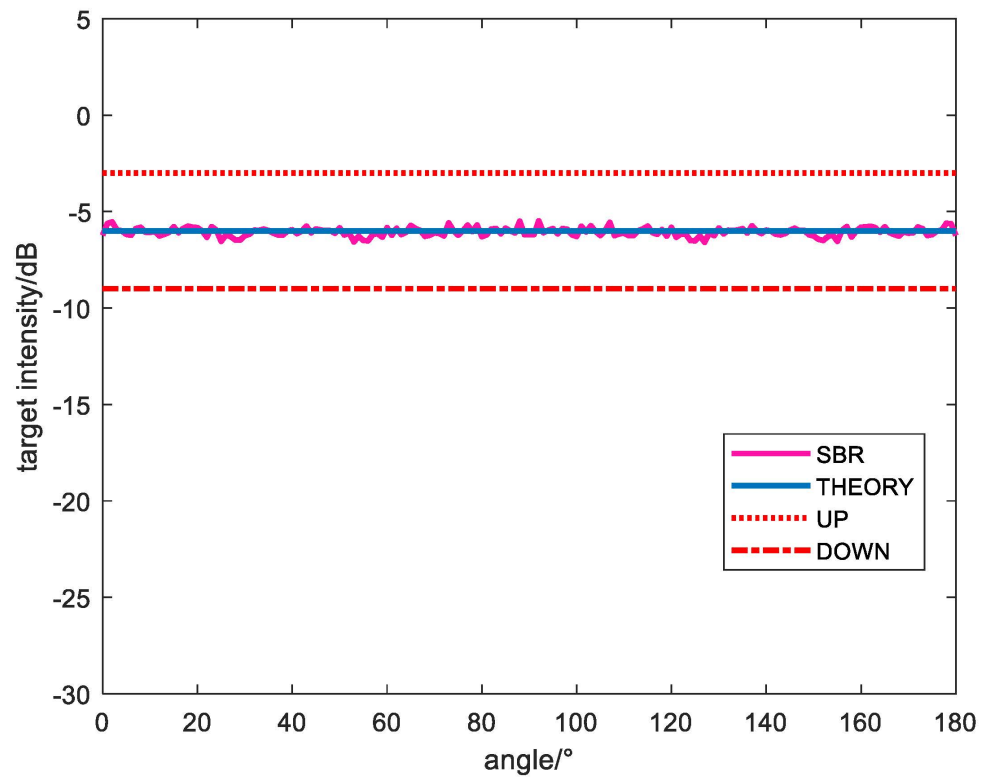


Figure 7. Sphere angle-intensity curve.

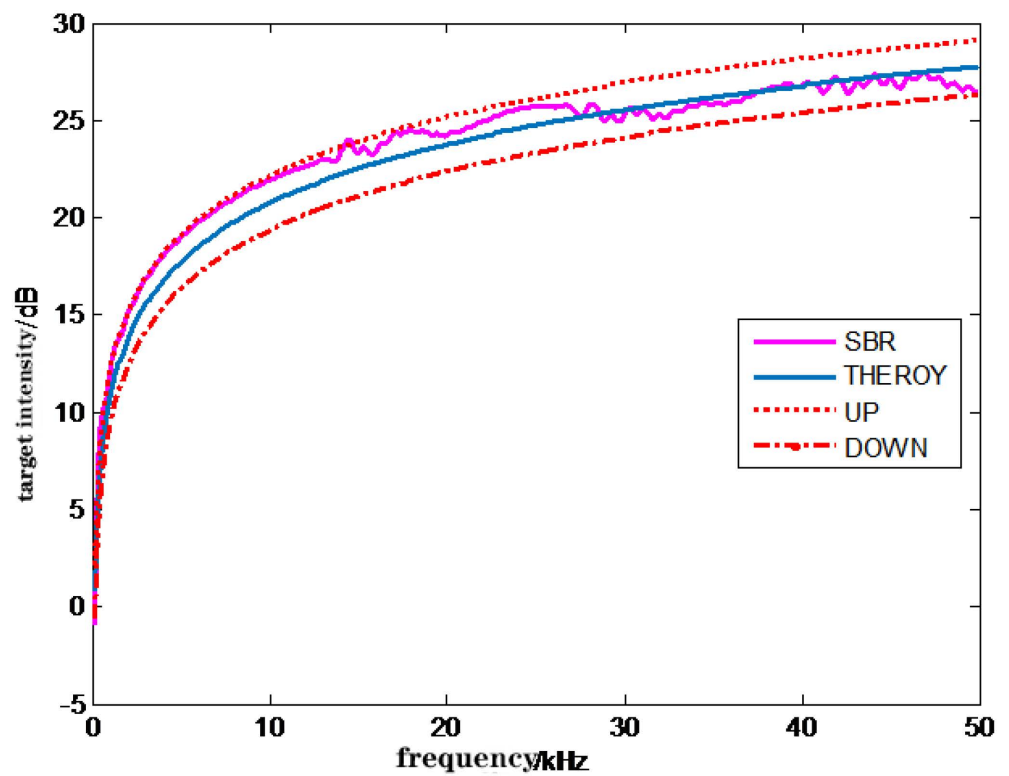


Figure 8. Cylindrical frequency-intensity curve.

## (b) Verification of validity

The 1 m radius sphere model shown in Table 1 was used as the object to verify the effectiveness of the algorithm. According to Table 1, at this time, the meshing precision of the sphere model surface element was 0.05 m, and the aperture of the acoustic beam pipeline was set as 0.01 m and 0.005 m, respectively. Plane frequency scanning was carried out on the sphere model, and the calculated results of the target intensity were shown in Figure 9. According to the analysis of Figure 9, as the incidence wave frequency increases, its wavelength becomes shorter, the meshing accuracy of the surface element of the incident wavelength becomes lower, and the fluctuation of the calculated results increase. However, the results of the fluctuation can be significantly suppressed by reducing the pipeline aperture of the low beam to reduce the proportion of the pipeline split during GA calculation. Thus, it is proved that the TD-ASBR algorithm can be effectively applied to the bandwidth signals in a certain frequency band through the corresponding adjustment of the surface element grid and the pipeline aperture of the acoustic beam.

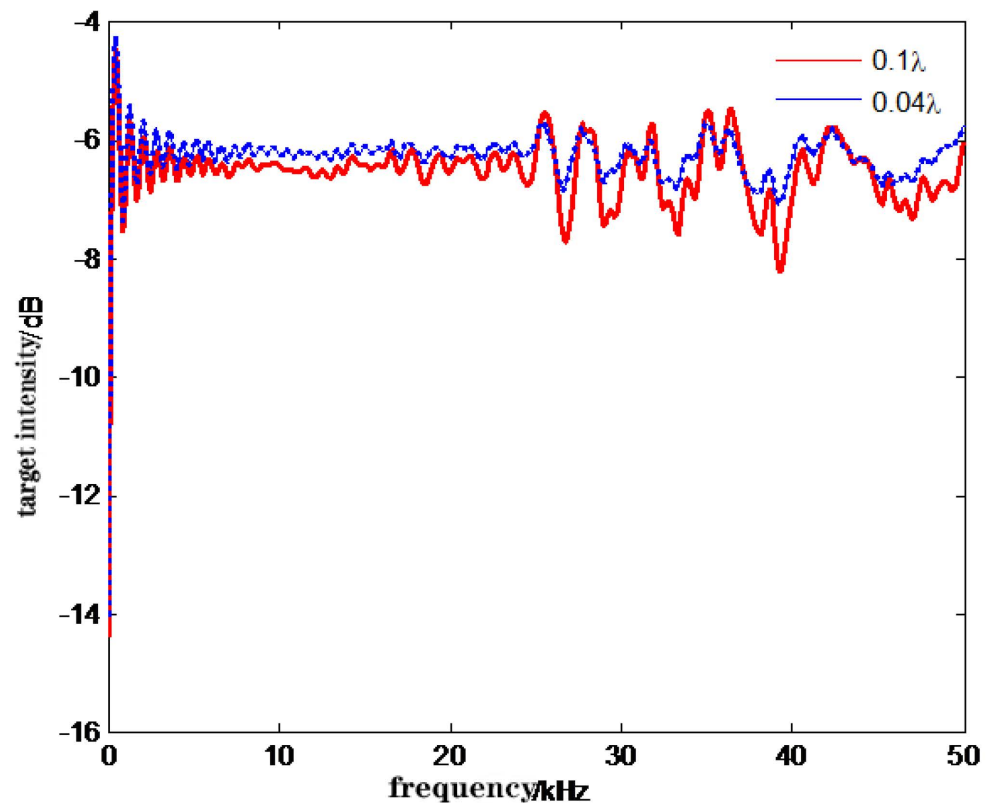


Figure 9. Sphere frequency–intensity curve.

## (c) Verify information completeness

TD-ASBR method is used to generate the time domain echo simulation signals of the model targets listed in Table 1, such as sphere, cross column and Benchmark submarine, as shown in Figure 10. Acoustic ISAR imaging results of the above time domain echoes are shown in Figure 11.

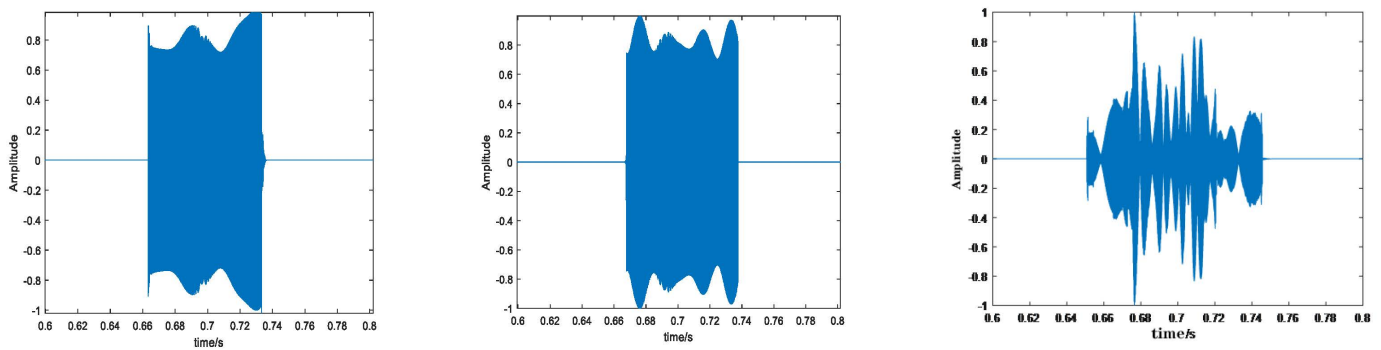


Figure 10. Time domain echo signals of different targets.

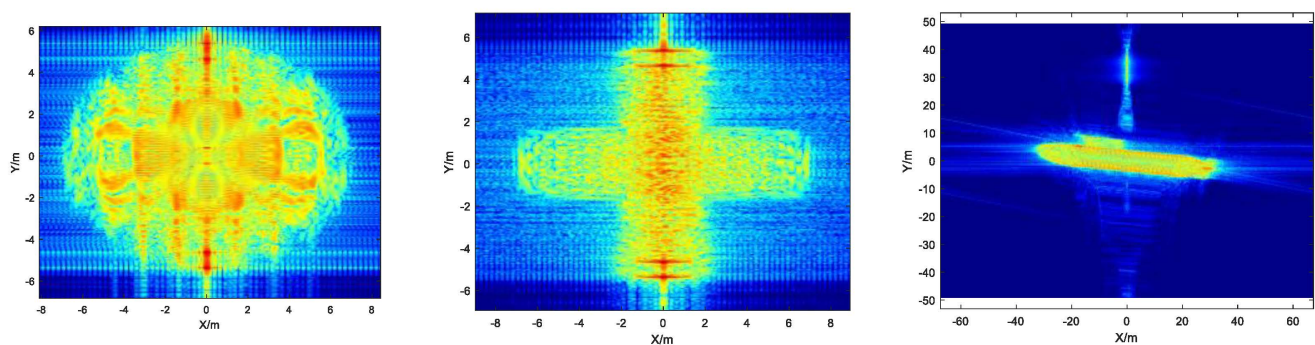


Figure 11. ISAR imaging results of the time domain echo signals of different targets.

In addition to echo delay, the Doppler frequency modulation, phase lag and other time-domain echo simulation signals usually contain one-dimensional information, the acoustic ISAR imaging results can accurately reflect the shape, size and spatial distribution characteristics of the target model, and intuitively prove that the simulation signals generated by the TD-ASBR method have higher completeness

#### (d) Analysis of classical submarine target echo

The pipeline division accuracy is 0.005 m. Under the LFM pulse incidence condition, the conventional integral dimension reduction method is adopted to calculate the target echo in the time domain of the Benchmark submarine at different incidence angles and can carry out the time-domain correlation analysis. The results are shown in Figure 12. Calculate the circumferential TS value of the Benchmark submarine with the step size of  $1^\circ$  and draw the butterfly diagram of the target intensity, as shown in Figure 13.

The results of the time-domain correlation analysis shows that the TD-ASBR method is effective for the conventional target multi-spot detection algorithm, and the distribution characteristics of the radial bright spots are consistent with the target azimuth-direction. Additionally, the intensity of the submarine target butterfly figure has also expressed the right kind of typical characteristics of the target; the whole is within the range of  $360^\circ$  circumferential distribution is axisymmetric, but on both ends of keel not only strength rapidly decreases, and especially the boat stem from the location to the influence of the podium and balanced rudder, a small angle change will cause the larger ups and downs of the target strength. The results of these classical analysis methods further prove the effectiveness and reliability of the TD-ASBR method.

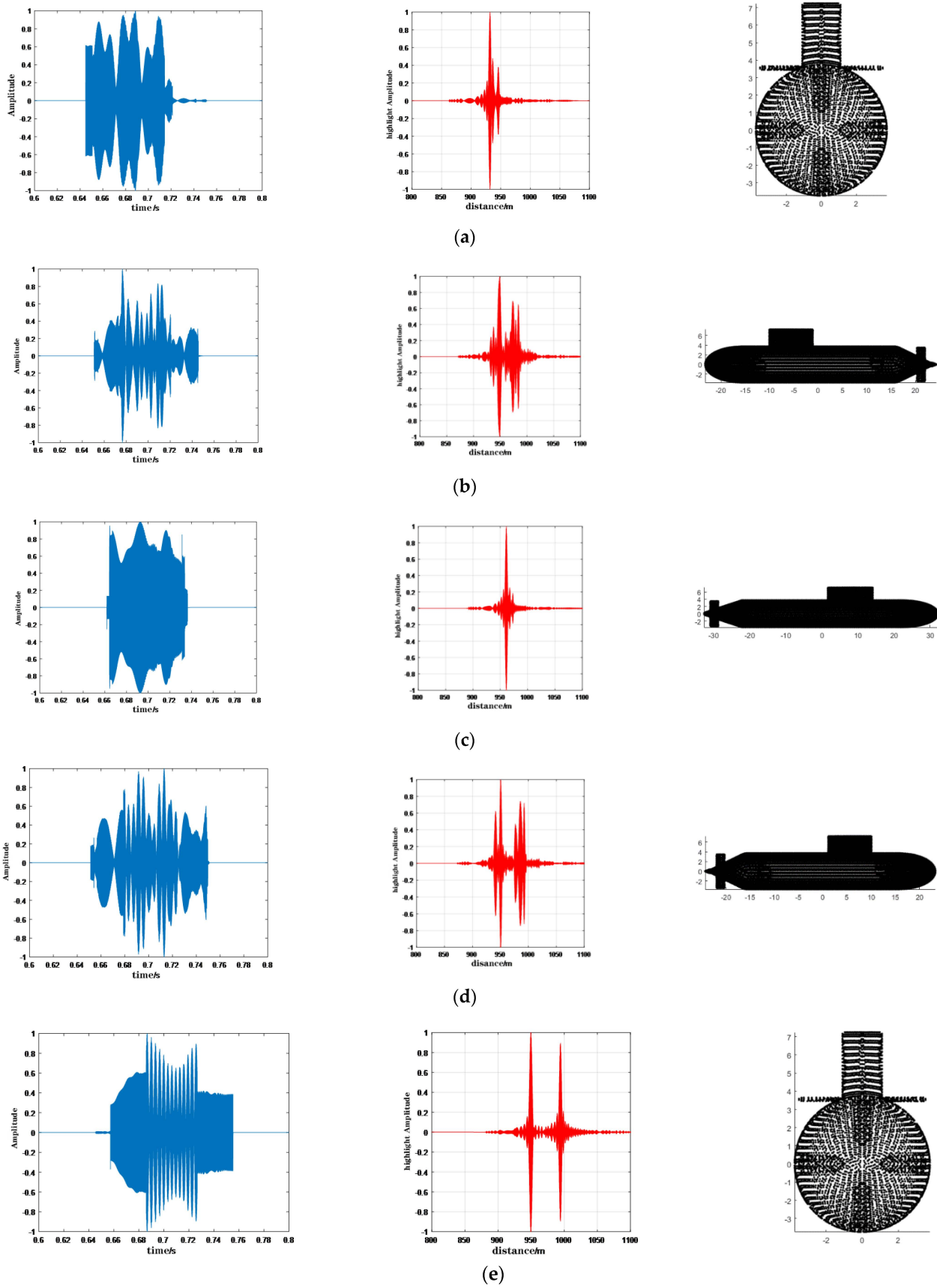


**Figure 12.** Time domain echo and highlight correlation analysis of linear frequency modulation (LFM) signal. (a) 0 degree; (b) 45 degree; (c) 90 degree; (d) 135 degree; and (e) 180 degree.

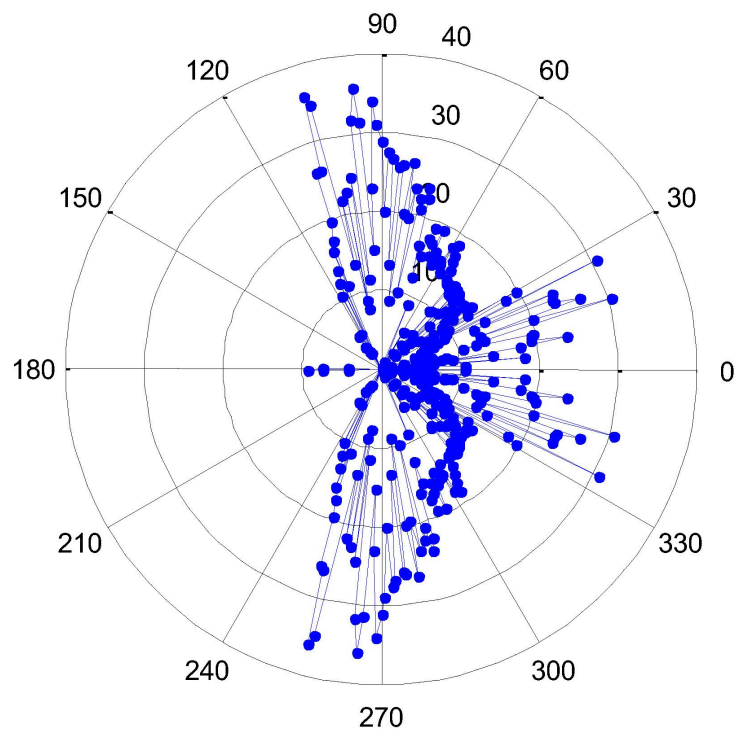


Figure 13. TS butterfly chart of the benchmark submarine.

### 7.3. Analysis of PA Acceleration Results

To improve the efficiency of the simulation calculation, this paper proposes a simplified accelerated calculation method for the PA integral. For the Benchmark boat, the PA acceleration algorithm and conventional integral dimension reduction method are, respectively, adopted to carry out simulation echo calculation. The comparison of the calculation results of the single-side target strength is shown in Figure 14.

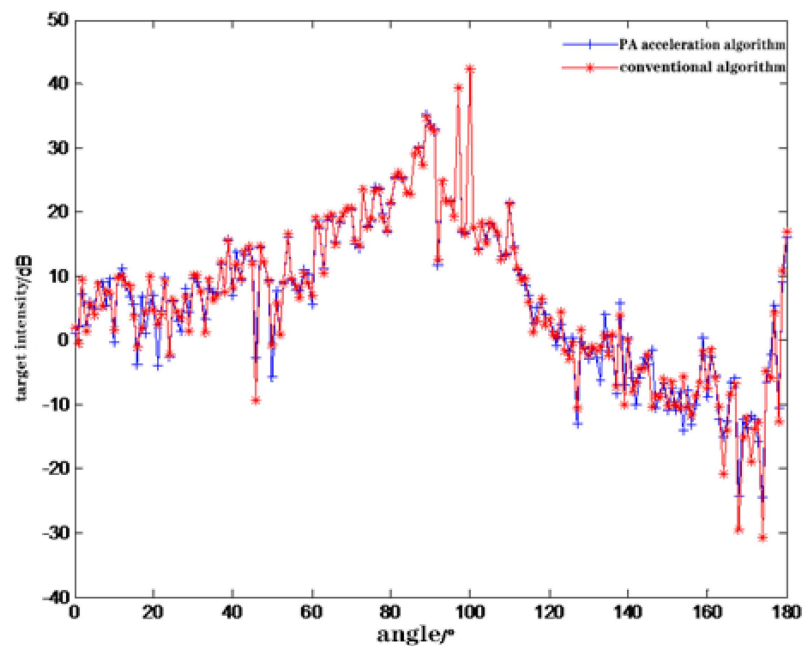


Figure 14. Comparison of the PA acceleration algorithm and conventional integral dimension reduction results.

For the standard bodies, such as ball, column and standard boat, the PA acceleration algorithm and conventional integral dimension reduction method are, respectively, used for the calculation, and the calculation time-consuming comparison is shown in Table 2.

**Table 2.** Comparison of the calculation time (unit: seconds).

Algorithm	Entity Model	Ball (0.05 $\lambda$ )	Column (0.05 $\lambda$ )	Standard Boat (0.1 $\lambda$ )
GPU-PA acceleration algorithm		0.65	0.35	2.69
GPU-Conventional integral dimension reduction		4.45	1.46	9.20
accelerative ratio		6.84	4.17	3.42

The results in Figure 14 and Table 2 show that the computational efficiency of the TD-ASBR method accelerated by PA can be significantly improved under the condition of abandoning a certain solving accuracy. This point will provide strong support for the smooth solution to the problem when the underwater target echo simulation is larger and more complex than that of the Benchmark boat.

## 8. Conclusions

To solve the needs of the accurate simulation of complex underwater target echoes quickly, this paper, based on the derivation of the time-domain Kirchhoff integral formula, first defined the solution vector and used the Stokes formula to reduce the dimension of the two-dimensional integral process, which effectively reduces the computational complexity of the integral and provides a theoretical basis for the parallel solution of the time-domain simulation echo. At the same time, combined with the geometric acoustic method (GA), based on the KD-tree spatial partitioning algorithm, which has mature application in computer graphics, through modeling and analysis of several key problems affecting the calculation of the sound field in the process of the geometric tracking of sound lines, and finally established the efficient parallel characteristics. The acoustic bouncing ray calculation method (TD-ASBR) for the time domain target echo simulation. In the realization of the simulation examples, the TD-ASBR method was used to simulate the angle-intensity and frequency-intensity responses of typical models, such as sphere and cylinder, and the correctness and effectiveness of the method are analyzed and verified. At the same time, the acoustic ISAR imaging method is used to directly prove that TD-ASBR method generates target echo simulation results with more complete target information. The comparison of the echo simulation results of the PA acceleration method shows that TD-ASBR can provide a corresponding simulation solving efficiency under different simulation accuracy conditions. The results of the TD-ASBR method proved to be accurate and reliable. The algorithm can be accelerated by the high-performance parallel computing platform, which has high parallel computing efficiency and is suitable for the broadband fine echo simulation of complex underwater targets.

It can be seen from the design process of the TD-ASBR method that the algorithm is more suitable for high-frequency acoustic conditions. However, although not to the low frequency under the condition of effective elastic echo simulation, for the calculation of surface acoustical material laying conditions, will be certain to approximate simplified, acoustic pulse is obtained by using the layered medium acoustic spread across the medium state and still use the TD method of ASBR processing, which is a direction for further research.

**Author Contributions:** Conceptualization, G.Z. and X.W.; methodology, G.Z. and N.S.; software, S.S. and X.W.; validation, W.Z.; formal analysis, G.Z. and X.W.; writing—original draft preparation, G.Z. and X.W.; visualization, N.S.; funding acquisition, X.W. All authors have read and agreed to the published version of the manuscript.

**Funding:** This work was funded in part by the China Postdoctoral Science Foundation (2013M540735); in part by the National Nature Science Foundation of China under Grant 61901388, 61701360; and in part by the Fundamental Research Funds for the Central Universities.

**Institutional Review Board Statement:** Not applicable.

**Informed Consent Statement:** Not applicable.

**Data Availability Statement:** Not applicable.

**Conflicts of Interest:** The authors declare no conflict of interest.

## References

1. Tang, J.; Bai, Y.; Yan, L.; Wang, W. GMA phased array for active echo control of underwater target. *Appl. Acoust.* **2022**, *190*, 108646. [[CrossRef](#)]
2. Wang, B.; Wang, W.-h.; Fan, J.; Zhao, K.-q.; Zhou, F.-l.; Tan, L.-w. Modeling of bistatic scattering from an underwater non-penetrable target using a Kirchhoff approximation method. *Def. Technol.* **2022**, *18*, 1097–1106. [[CrossRef](#)]
3. Wang, J.; Jia, B.; Zhang, Y.; Wang, R.; Wu, J.; Wang, Z.; Zhu, Y. Similarity measurement of underwater complex model simulation and acoustic image test. In Proceedings of the 6th International Conference on Communication, Image and Signal Processing (CCISP), Chengdu, China, 19–21 November 2021; pp. 7–10.
4. Zhang, Y.L.; Wang, Y.M.; Huang, A.P.; Hu, X. Study on reflection characteristics of underwater target and laser echo power. *Optoelectron. Lett.* **2020**, *16*, 137–142. [[CrossRef](#)]
5. Zhou, Y.; Wen, W.; Han, J.-H.; Yang, R.-J. Research on Acoustic Scattering of Underwater Complicated Target Based on Sound-Solid Coupling. *J. Unmanned Undersea Syst.* **2020**, *28*, 051–056.
6. Tang, W.-L. Calculation of Acoustic Scattering of a Nonrigid Surface Using Physical Acoustic Method. *Acta Acust.* **1993**, *18*, 45–53.
7. Kim, K.; Jin-Hyeong, K.; Cho, D.; Seong, W. Applying time domain physical optics to acoustic wave backscattering problem. *Appl. Acoust.* **2010**, *71*, 321–327. [[CrossRef](#)]
8. Houshmand, B.; Chew, W.C.; Lee, S.W. Fourier Transform of a Linear Distribution with Triangular Support and Its Applications in Electromagnetics. *IEEE Trans. Antennas Propag.* **1991**, *39*, 252–254. [[CrossRef](#)]
9. Sun, N.W.; Li, J.C.; Wan, Y.M.; Zhao, G.; Lv, W.; Fan, R.N. Simulation of Submarine Target Strength Forecast Based on Improved Planar Element Method. *Torpedo Technol.* **2016**, *24*, 254–259.
10. Gordon, W.B. Far Field Approximations of the Kirchhoff-Helmholtz Representations of Scattered fields. *IEEE Trans. Antennas Propag.* **1975**, *23*, 590–592. [[CrossRef](#)]
11. Zhang, X.-G.; Zhang, J.-F.; Lü, S.; Cao, F.; Li, G.-J.; Wang, N. Rapid Method for Large-scale Target Sound Scattering Calculation and Experiment Validation. *J. Ship Mech.* **2020**, *24*, 409–418.
12. Shen, N.; Wei, B. TDSBR Algorithm Based on Analytic Integral and its Application in Scattering Problems. *Chin. J. Radio Sci.* **2017**, *32*, 712–717.
13. Jian-Jun, D.; Lei, C.; Zhi-Wei, L.; Ru-Shan, C. Analysis of Electromagnetic Scattering of Electrically Large Objects with Time Dominant Shooting and Bouncing Rays Method. *Syst. Eng. Electron.* **2010**, *32*, 1846–1849+1888.
14. Jeng, S.-H. Near-field scattering by physical theory of diffraction and shooting and bouncing rays. *IEEE Trans. Antennas Propag.* **1998**, *46*, 551–558. [[CrossRef](#)]
15. Ji, J.-Z.; Liu, Z.-H. Electromagnetic Occultation Algorithm Based on Facets Group and Optimization. *J. Beijing Univ. Aeronaut. Astronaut.* **2009**, *35*, 453–456.
16. Sivaks, E.; Lischinski, D. Review: Kd-tree Traversal Algorithms for Ray Tracing. *Comput. Graph. Forum* **2011**, *30*, 199–213. [[CrossRef](#)]
17. Lozano, L.; Gutiérrez, O.; Cátedra, M.F. Comparison Between PO-GO, GO-PO and PO-PO Applied to Calculate the Contribution of the Double Reflection Between Flat Patches. In Proceedings of the 2006 IEEE Antennas and Propagation Society International Symposium, Albuquerque, NM, USA, 9–14 July 2006.